Pulsed multiampere source of negative hydrogen ions

Cite as: AIP Conference Proceedings **111**, 363 (1984); https://doi.org/10.1063/1.34436
Published Online: 29 May 2008

Yu. I. Bel'chenko, and G. I. Dimov

PULSED MULTIAMPERE SOURCE OF NEGATIVE HYDROGEN IONS

Yu. I. Bel'chenko and G.I. Dimov
Institute of Nuclear Physics
Novosibirsk 90, U.S.S.R.

ABSTRACT

A description is given of a pulsed model of a multiampere honeycomb surface plasma source of negative hydrogen ions (H^-). The H^- emitter is the cesium-coated cathode surface in a high-current, glow discharge; the surface consists of a large number of spherically concave indentations. The concavity of the emitting surface of the indentation and of the adjacent cathode sheath, where ions are accelerated, ensures two-dimensional geometrical focusing and a 20-fold compression of the H^- stream from a larger part of the cathode surface into the emission slits of the multiaperture extraction system. A pulsed (0.2 to 0.8 ms) H^- beam carrying a current in excess of 11 A was produced from 600 indentations with an emitting surface area of ~60 cm^2 and accelerated to 25kV. The gas efficiency of the source was $\gtrsim$20%. The thermal loads on the electrodes were <1 kW/cm^2.

INTRODUCTION

The injection of fast hydrogen atoms is one of the main methods of storing, heating, and controlling the distribution of particles in the plasma of thermonuclear devices. In existing injection systems, atoms having an energy of ~100 keV/nucleon are produced through neutralization of positive ions. As the particle energy is increased to the range of 200 keV to 1 MeV in injectors of the next generation, neutralization by stripping of negative ions must be used. In contrast to positive ions, such negative ions have at these energies a high neutralization efficiency (80%-100%) in a plasma target[1] or a laser target.[2]

In recent years work has been done to develop high current negative-ion sources as well as efficient neutralizers for such high energy injectors. In addition to traditional charge exchange sources[3,4] and volume sources of negative ions,[5,6] which are experiencing their second birth, intensive studies are under way on new types of sources: surface conversion sources[7] and surface plasma sources.[8-16] Surface-plasma sources (SPS) have already been developed that allow the production of pulsed H^- (D^-) beams with a current of several amperes;[11-13] negative beams with a current of 0.7-1.1 A have been produced and accelerated from quasi-steady-state SPS.[15,16]

In an SPS the plasma sheath adjacent to the emitter of secondary ions (the cathode) delivers to the emitter surface intense fluxes of ~100 eV ions and atoms (Fig. 1). Upon collision with the surface, primary ions and atoms are partially reflected and sputter hydrogen particles adsorbed on the emitter. Due to a surface work function reduced to ~1.5 eV by cesium adsorption, a significant fraction of

0094-243X/84/1110363-13 $3.00

fast particles leaving the emitter escapes beyond the surface potential barrier in the form of negative ions.[17] These negative ions are accelerated in the sheath of potential next to the electrode and after passing through the plasma, enter the beam-forming region.

SPS with geometric focusing are promising for use in controlled thermonuclear fusion. In these SPS the negative ion emitting surface has the form of concave semicylindrical grooves or spherical indentations (Fig. 1B).

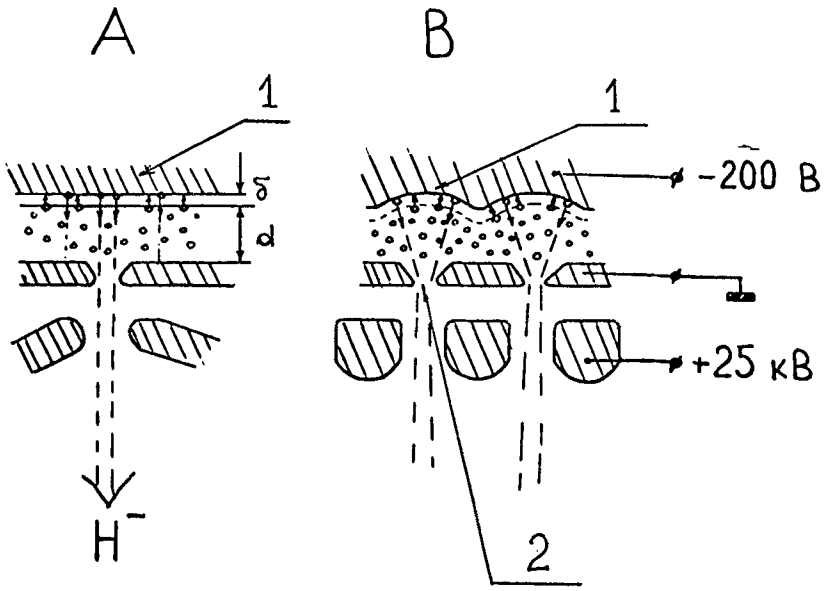

Fig. 1. Scheme of the surface-plasma method of generating negative ions. (A) with plane electrode geometry (a planotron). (B) with geometrical focusing: [1] cylindrically or spherically concave cathode indentations, [2] slit-type or round emission apertures.

As a result, the negative ions accelerated in the sheath are focused from the concave surface of the emitter into relatively small emission slits or apertures. Because of a high compression of the negative-ion stream into the emission holes, up to 80% of the working surface of the cathode can be used in SPS with geometric focusing. The reduction of the relative area of the emission slits (by a factor of 3-5 in SPS with grooves and by a factor of 10-20 in honeycomb SPS) makes possible a significant decrease in hydrogen and cesium consumption and a 10-20% gas efficiency for reduced discharge power and thermal loads of ~1 kW/cm^2 on the electrodes.

One dimensional geometric focusing was first implemented in semiplanotron sources[10,11] and is being used successfully in other SPS modifications: in a ring source,[12] in a magnetron with

grooves,[13] and a multicusp source.[15] Two-dimensional geometric focusing has been tested in a small honeycomb SPS[14] and also is used in the multiampere honeycomb source (MHS) described below, which has a much larger emitter surface.

DESIGN OF THE SOURCE

A diagram of the multiampere honeycomb source (MHS) is presented in Fig. 2. The high current glow discharge, with an open electron drift, is localized in the gap between the cathode emitting surface 1 and the anode cover 2 with emission holes. At the edges the discharge space is limited by side projections 1a and 1b of the cathode, by the ignition gap 3, and by the electron-dump region (not shown in Fig. 2).

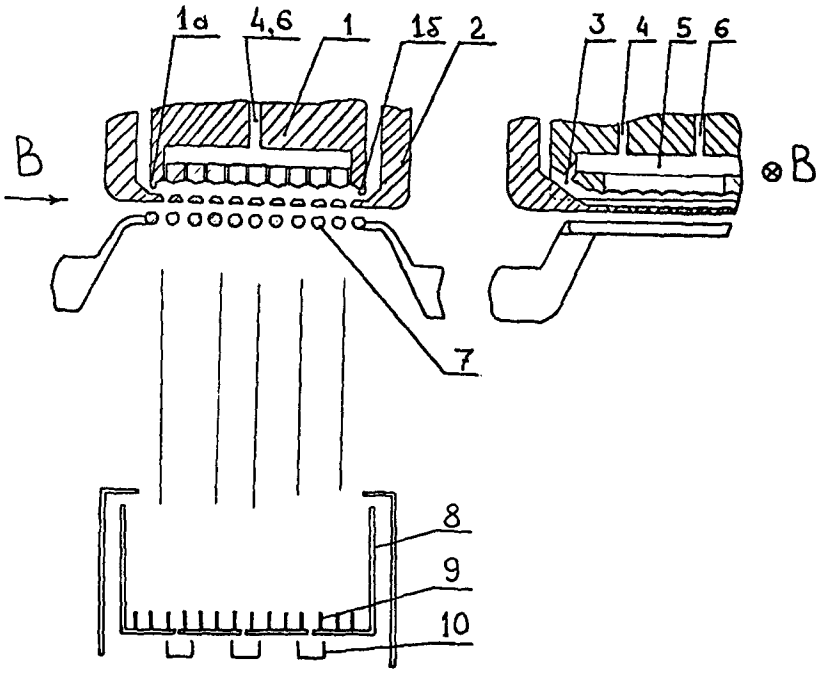

Fig. 2. Diagram of a honeycomb source. At left - view along the magnetic field; at right - across the magnetic field. (1) cathode; (1a and 1b) side projections of cathode; (2) anode body; (3) ignition gap; (4,6) H_2 and Cs supply channels; (5) distributor cavity in cathode; (7) extractor electrode; (8) Faraday cup for measuring the total negative ion current; (9) fins for intercepting secondary electrons (10); Faraday cup for measuring current density over the beam cross section.

A magnetic field of 0.5-1.5 kG is generated parallel to the plane of the discharge gap by means of an electromagnet and special pole tips. The magnetic field causes oscillations of the electrons in the space between the side projections of the cathode, and also attenuates and removes from the beam electrons extracted together with the negative ions. The width of the zone of electron oscillations between the side projections of the cathode is 3 cm, and the thickness is 1-2 mm.

In the ignition gap of the cathode, the height of the side projections of the cathode has been increased to 4-5 mm, thereby improving electron confinement in the oscillation zone and lowering the initial hydrogen density in the ignition gap that is required to maintain a self-sustained discharge. The loss of plasma from the ignition gap due to electron drift in the crossed E x B fields of the electrode gap helps the propagation of the discharge over the entire electrode gap, which is 20 cm long. The discharge current was varied in the range of 0-700 A, the discharge voltage was in the range 150-200 V under operating conditions, and the discharge pulse length was varied from 300 μs to 2 ms.

Hydrogen is supplied to the discharge chamber by means of pulsed electromagnetic valves through special channels (4) and the cavity (5) inside the cathode, which is connected to the main chamber by narrow (~0.05 mm) slits. A distributor plate with a variable number of bypasses is installed in the inside cavity of the cathode to ensure the required hydrogen density profile over the length of the discharge gap (the plate is not shown in the figure).

Cesium is supplied to the ignition gap and to the cathode surface from independently heated containers holding a mixture of cesium chromate and titanium and located outside the source. Supply is accomplished via channels 6 and through the inside cavity of the cathode.

The emitting surface of the cathode has dimensions of 3 x 18 cm^2 and consists of ~600 spherical, concave indentations arranged on the cathode surface in orthogonal or hexagonal matrices (Fig. 3). To ensure more complete utilization of the cathode surface, the indentations overlapped, i.e., their diameter was greater than the distance between the centers of adjacent rows and the boundaries between neighboring cells created either a square or honeycomb structure (Fig. 3). The radius of curvature of indentations within a square structure was 3 mm, and the distance between the centers of rows of adjacent craters was 3 mm. Indentations with a 3.5 mm radius of curvature were used in the honeycomb structure.

The cathodes were made from plates of monocyrstalline molybdenum. This material sputters lightly, has a low probability of forming arc spots, and, in contrast to tungsten, has a better adsorption of cesium from the flux of cesium ions and atoms incident on the cathode. Forced cooling of the electrodes was not used in the pulsed source described here. Conditioning and outgassing of the electrodes at the start of the working cycle were accomplished with pulsed low current glow discharges. Switching the source to a high current glow discharge operation was speeded up significantly

when the cathode was heated to 400°C by the heater built into its cavity (the heater then was shut off).

Conical emission holes with a 0.9 mm diameter were drilled at the negative ion focusing points on the anode cover (allowing for the displacement due to the magnetic field of the source). The accuracy of the alignment of cathode indentations and emission apertures was checked by the sputtering marks that appeared on the anode cover at negative ion focusing points after the source was run.

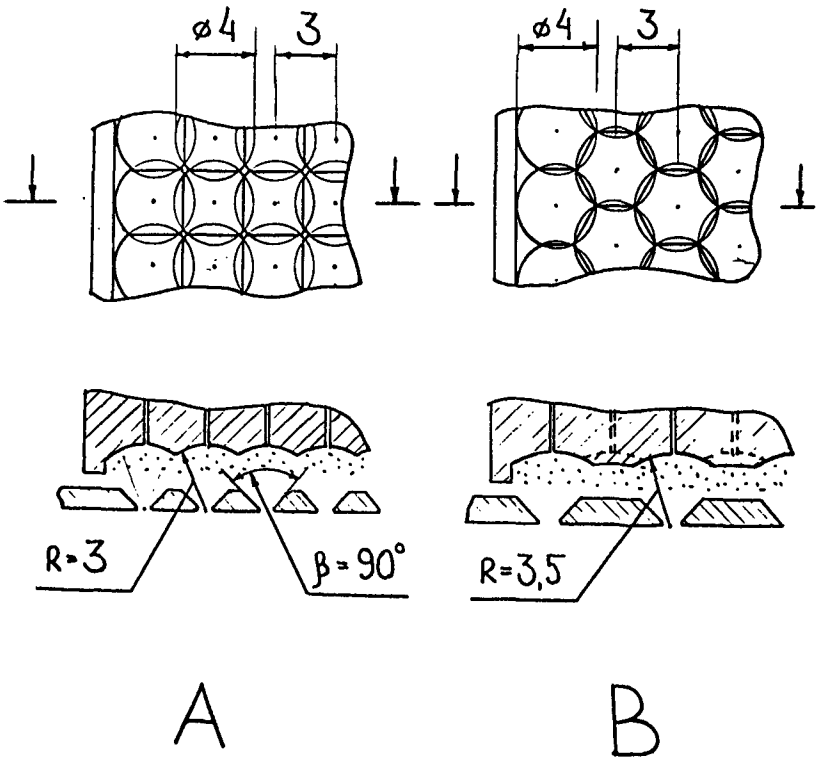

Fig. 3. Arrangements of spherically concave indentations on the cathode surface. (A) orthogonal arrangement; (B) hexagonal arrangement.

The negative ions emerging through the emission holes are extracted by supplying a pulsed voltage (25 kV, 0.2-0.8 ms) to the body of the source. The electrodes of the multiaperture extraction system (7 in Fig. 2) are grounded through the current measuring resistor. To increase the dielectric strength of the extraction gap (1.3 mm long, with an area of 3.3 x 20 cm^2), the grid of the extraction electrode has been fabricated from profiled molybdenum and is heated by heaters built into the grid wires.

In the source being described, the electrons that enter the extraction gap as a result of diffusion from the plasma sheet as well as those formed on the cesium-coated walls of the emission slits and those formed by destruction of negative ions are accelerated to the full extraction voltage. The height of the trochoid of electrons drifting in the crossed E x B fields of the extraction gap exceeds the width of the extraction gap; therefore, the stream of accelerated electrons is intercepted by the extraction electrode and by the pole tips of the magnet.

The negative ion beam current and its density distribution were measured with Faraday cup collectors (8 and 10 in Fig. 2) located at a distance of 20-25 cm from the extraction region. Fins (9), intercepting secondary particles moving in the stray field of the source, serve to suppress the departure of secondary electrons from the large collector. Separate measurements were made of the current on the extractor grid and of the total current in the extractor circuit. In addition to the H^- beam current, the total current included the flux of electrons and other negative particles. A mass analysis of the extracted negative ion beam was performed by means of an additional magnetic analyzer with an entrance slit 20 mm^2 in area, that could be moved across the negative ion beam. Measurements of the source gas efficiency were made by using noise-immune fast ionization detectors that register both the total flux of hydrogen particles and the slow thermal component of the hydrogen flux emerging from the source.

The cesium density in the source and the cesium consumption were determined by means of a surface ionization type cesium detector.

CHARACTERISTICS OF THE SOURCE

The main factors that determine the efficiency of negative ion production in high current sources are the thickness and uniformity of the cesium coating of the cathode, the hydrogen density profile over the discharge gap, and the uniformity of the distribution of the discharge current (especially the ion current) over the cathode emitting surface.

When these factors were optimized, a pulsed beam of H^- ions with a current in excess of 11 A was produced from the source and accelerated to 25 keV. The total negative ion current recorded (allowing for heavy negative ions) reached 12 A, and the current in the extraction circuit was $\leq$ 25A. The H^- yield was proportional to the discharge current (curve I in Fig. 4a). For comparison, Fig. 4a shows the analogous relationship (curve II) for a small honeycomb source.[14] Figure 4b shows the dependence of the H^- current density, averaged over the beam cross section, on the average cathode current density for the MHS and for a small honeycomb source. Conversion efficiency of the discharge current into an H^- beam, $\alpha = j_-/\langle j_d \rangle$, of about 2% was achieved with discharge current densities of 8 A/cm^2 on the cathode of the MHS.

A typical negative ion current density distribution along the source is shown in Fig. 5. The drop in the negative ion emission at

the edges of the source was due to the reduced density of the plasma in those regions of the discharge. Over the flat part of the H^- current density distributions in Fig. 5, the conversion efficiency of the cathode current into the H^- beam current ($j_-/\langle j_d \rangle$) reaches a value of 2.7%, which is approximately half the value attained in a honeycomb source with a relatively small beam cross section.[14] This may be due to a higher current density in the regions of the cathode surfaces from which H^- ions are not extracted.

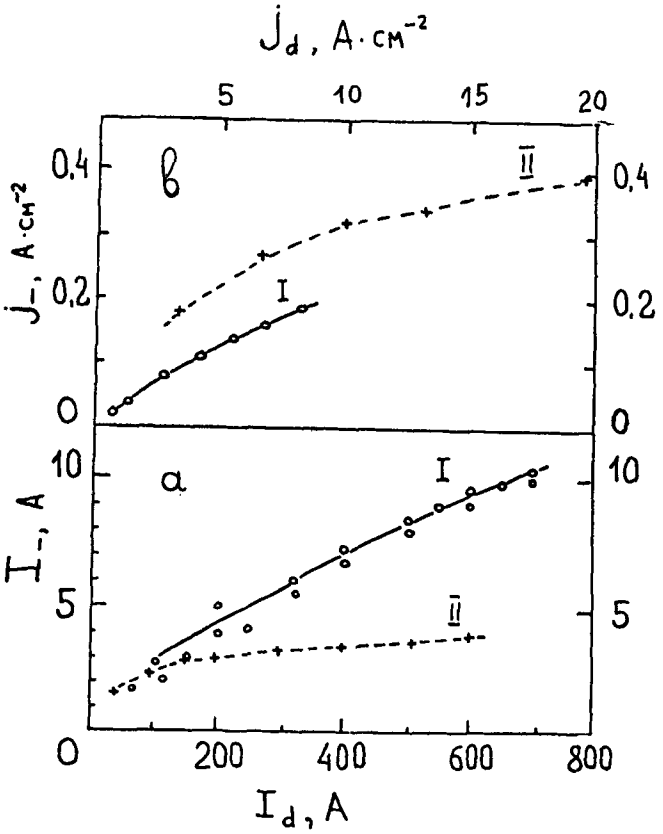

Fig. 4. (a) Dependence of H^- current I_- on discharge current I_d; (b) dependence of average H^- current density j_- in the beam on discharge current density j_d on the cathode (I - multiampere honeycomb source; II - small honeycomb source).

A magnetic analysis of the composition of the accelerated negative ion beam showed that heavy (O^-, etc.) impurity ions comprise 10-20% of the total beam current for discharge currents of $\leq$200A. During the beginning phase of the heating of the cesium chromate, the heavy ion component may amount to 40-50% of the beam current.

In the range of discharge currents 400-700 A, the extracted beam is 95-99% H^- ions (averaged over the pulse); the heavy ion component is substantially lower at the end of the discharge pulse than at the beginning. This fact may be explained by the removal of impurities from the cathode surface during ion bombardment. The cesium chromate (C_2CrO_4) used in the source was the main source of oxygen.

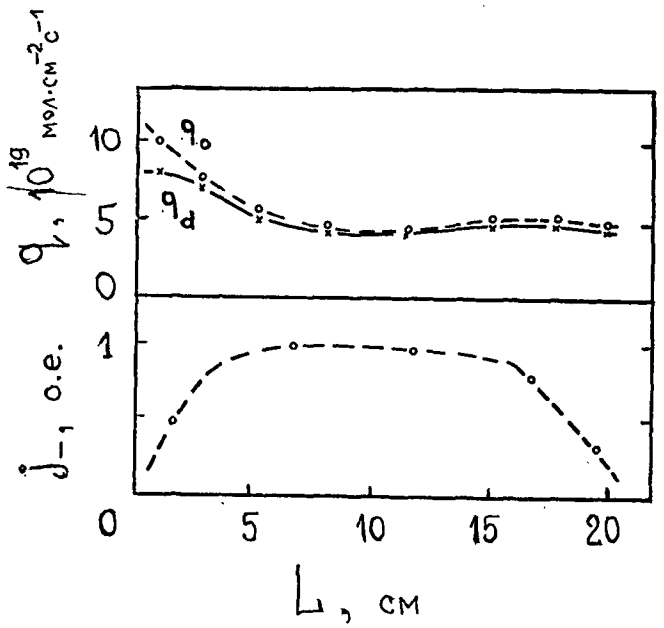

Fig. 5. Distribution of the density of the hydrogen flow from the source emission apertures (q_0 - before triggering of discharge, q_d - during discharge) and of the negative ion current density j_- over the length of the source across the magnetic field; L - distance from the ignition gap.

In the investigated range of discharge currents (<700 A), the loss of H^- ions in the plasma sheet, which was due mainly to collisions with plasma electrons, was small. The thickness of the plasma sheet of the high current source did not exceed 5×10^{12} cm^{-2}; accordingly, the transmission coefficient for negative ions during motion through the source plasma had the following value:

$$\mu_e = \frac{j_-}{j_-^0} \approx \exp\left(-n_e d \frac{\langle \sigma_e \upsilon_e \rangle}{\upsilon_{H^-}}\right) \geq 0{,}9$$

(σ_e is the cross section for H^- ion loss in collisions with electrons; the other notations are standard).

In the MHS the hydrogen density required to initiate a high current discharge depended on the magnetic field, the cesium concentration, the height of the side projections of the cathode, and other factors. Under the operating conditions of the source the initial hydrogen density in the ignition gap was ~3 x 10^{15} molecules/cm^3; the discharge propagated into the main part of the gap at a gas density of $\gtrsim 6 \times 10^{14}$ molecules/cm^3. A typical density distribution of the stream of hydrogen particles from the emission slits along the source before and during discharge is shown in Fig. 5. In contrast to SPS with a dense plasma,[18] in this source the total flux of hydrogen particles from the emission holes decreased insignificantly when the discharge was initiated (Fig. 5). The flux of hydrogen particles Q_d emerging from the source during the discharge pulse consisted of H^- ions, fast H^0 atoms, and a slow component: thermal hydrogen molecules and atoms. When the H^- ion beam current was $I_- = 11$ A, the total flux of hydrogen particles from the source was (converted to atoms) $Q_d = 3 \times 10^{20}$ atoms/s; accordingly, the pulsed gas efficiency of the source was $\eta = I_-/Q_d \gtrsim 20\%$. Because of the pumping effect of the plasma sheet,[18] the slow component of the hydrogen flux from the source decreased 30-40% from the initial value when a high current discharge was triggered. Model experiments using a scaled-up discharge chamber and a geometry similar to a cell of the high current source showed that when the thickness $n_e d$ of the sheet of the discharge plasma increased in the range 10^{12} to 2 x 10^{13} cm^{-2}, the flux of thermal hydrogen from the chamber decreases exponentially with a constant $n_e\lambda \cong 8 \times 10^{12}$ cm^{-2}. Reduction of the density of H_2 molecules in the discharge chamber and in the extraction region is important for eliminating the additional loss of negative ions upon collisions with H_2 molecules. Such losses were insignificant in this source because of the reduced H_2 density in the main portion of the discharge gap and a small flow of H_2 molecules into the extraction region. (This flow was small because of the small area of the emission holes.) The attenuation of the H^- ion stream due to ion losses on hydrogen molecules during the transit from the source cathode to the collector (~20 cm) was:

$$\mu_{H_2} = \exp - \langle \sigma_{H_2} n_{H_2} Z \rangle \simeq \exp - \left(4 \times 10^{-16} \cdot n^{\circ}_{H_2}\right) \simeq 0{,}8$$

(σ_{H_2} is the H^- loss cross section for collisions with H_2; n_{H_2} is the hydrogen density in the discharge chamber; and Z is the coordinate in the direction of motion of an H^- ion). Let us note that as the number of cells increases, so too do the total flux and the effective thickness of the "cloud" of hydrogen molecules that destroys negative ions, $\int_0^\infty n_{H_2}\, dZ$. This cloud emerges from the emission holes and is pumped through the extraction and beam forming regions. When a ribbon beam with an emission cross section a x b is extracted, the effective thickness increases linearly with an increase in the smaller transverse

dimension b and logarithmically with an increase in the large dimension a:

$$\int_0^{\infty} n_{H_2} dZ = n^{\circ}_{H_2} \cdot d_{H_2} + \left(n^{\circ}_{H_2} \frac{S_{em}}{a \cdot b}\right) \cdot b \frac{2}{\pi} \ln\left(\frac{\pi}{2} \frac{a}{b}\right)$$

where d_{H_2} is the total effective thickness of molecular hydrogen in the discharge chamber and emission holes.

The cesium coverage of the cathode is 2-4 x 10^{14} atoms/cm^2, which ensures high values of the coefficients of secondary negative ion emission $K^- \cong 0.2$-0.7 and of secondary electron emission $\gamma = 3$=6 in SPS[19]; it is regulated by the rate of supply of cesium to the discharge chamber and depends on the electrode temperature, the cathode current density, and other factors. The thickness N of the cesium coating is determined by the relationship between the rate j_{Cs} of arrival of particles on the surface and by the length of time τ the cesium spends on the surface:

$$\frac{dN}{dt} = \langle \alpha j_{Cs} \rangle - \frac{N}{\tau}$$

where α is the sticking coefficient of cesium.

In the intervals between discharge pulses the value of N depends on the thermal flux of cesium from the discharge chamber volume: $j_{Cs} = \frac{n_{Cs} \cdot \bar{\nu}}{4}$ (actually on the thermodesorption flux from the opposite surface) and on the rate of cesium desorption from the electrode: $N/\tau = N\omega_0 \exp(-W/kT)$. Optimum cesium coverage on molybdenum is maintained with a relatively low volume density of cesium, since the sticking coefficient α of cesium for the optimal coverage is close to 1, and the heat of desorption from an optimal layer on molybdenum is high: $W \sim 2$ eV. Because of the low volume density of cesium ($\lesssim 10^{12}$ atoms/cm^3) and the small area S_{em} of the emission holes, the cesium flux from the source in the intervals between discharge pulses is small: $Q_{Cs} = \frac{n_{Cs}}{4} \times S_{em} \cong 0.5$-$1 \times 10^{16}$ s^{-1}; hence the rate of required cesium supply compensating for this "thermodesorption" consumption is low.

When discharge is triggered, the cesium coverage of the source electrodes changes. The cesium adsorbed on the electrodes is sputtered by fast discharge particles; the coefficient of sputtering of cesium from an optimal coating on molybdenum increases with the energy and mass of the particles bombarding the surface, having a value of order 10^{-3} for 100 eV hydrogen ions. The cesium desorbed from the electrodes is ionized in the discharge chamber with a mean

free path of $\lambda_{Cs} = \nu_{Cs}/n_e \langle\sigma_{Cs}\nu_e\rangle$ (where σ_{Cs} is the cross section of ionization of cesium by electrons) and is returned to the cathode by the electric field of the discharge.[21] For plasma densities $n_e = 2 \times 10^{12}$ to 10^{13} cm^{-3}, the mean free path is λ_{Cs} = 1-0.2 mm. As measurements have showed, the total cesium flux onto the cathode during discharge is 2-3 orders of magnitude larger than the stream onto the anode, and it consists basically of Cs^+ ions. The thickness of the cesium layer on the cathode is determined by the sticking efficiency of cesium from the incident Cs^+ flux, which in turn depends on the cathode material, the thickness and structure of the cesium layer, the presence of surface contamination, and other factors. Because of a favorable atomic mass ratio, molybdenum adsorbs cesium well from the flux of ions. Thus, when a clean molybdenum surface is bombarded with 100-200 eV ions, only around 5% of the incident ions are reflected. The remaining 95% temporarily stick to the surface and fly off (~60%) in the form of slow cesium ions.[20] The cesium sputtering increases with increasing cesium coverage. This contributes to the rapid transport of cesium to cesium-depleted sections of the cathode both during startup of the source and during the discharge pulse.

In the MHS it is possible to obtain both, stable regimes with an optimal cathode coverage throughout the entire discharge pulse, and regimes with an increasing (or decreasing) cesium coverage of the cathode, by controlling the electrode temperature, the cathode current density, and the cesium supply rate. Because of the fast ionization of cesium in the discharge and its transport to the cathode, the loss of cesium through the emission holes of surface plasma sources during the discharge pulse is insignificant.

Let us present a summary of the basic parameters attained in the high current H^- source:

H^- beam current	- over 11 A
Heavy impurities (average over a pulse)	- <3%
Beam energy	- 25 keV
Beam pulse length	- 200-800 μs
Average emission current density of H^- ions in beam	- 180 mA/cm^2
Same, in the flat part of the distribution	- 220 mA/cm^2
Area of beam emission cross section	- 60 cm^2
Total current in extraction circuit	- ≦25 A
Number of indentations	- 600
Total operating surface of cathode	- 74 cm^2
Emitting surface of cathode	- 63.6 cm^2
Total area of emission apertures	- 3.86 cm^2
Gas efficiency (pulsed)	- at least 20%
Cesium consumption (due to loss between pulses)	- no more than 20 mg/hr
Discharge voltage	- 150-200 V

Discharge current	- 700 A
Average current density on cathode	- 9.5 A/cm^2
Thermal load on electrodes	- 1 kW/cm^2
Magnetic field in the discharge chamber	- 700-900 G

In conclusion let us take note of the properties of the MHS that are promising from the standpoint of its use in high energy neutral injectors for controlled thermonuclear fusion.

1. Low consumption of both the primary working material (hydrogen) and the secondary emission catalyst (cesium).

2. Shielding of 90% of the working surface of the cathode from direct impact of surface-damaging external fluxes of fast particles (positive ions accelerated in the extraction gap, etc.) through the emission holes.

3. A moderate level of power deposited on source electrodes; the possibility of heat removal by cooling in the steady state case.

4. The possibility of using a single source to obtain negative hydrogen ion beams of unlimited current with a high average emission density (~100 mA/cm^2) close to the average emission current density of high current positive ion beams.

Based on the pulsed source described here, we propose the creation of a quasi-steady-state version of a high current honeycomb source of H^- ions.

REFERENCES

1. G.I. Dimov, A.A. Ivanov, and G.V. Roslyakov. Fizika Plazmy, 6, 933 (1980).
2. J.H. Fink. Preprint UCRL-87301, Livermore, 1982.
3. N.N. Semashko, A.N. Vladimirov, V.V. Kuznetsov, et al. Inzhektory bystrykh atomov vodoroda (Fast Hydrogen Atom Injectors). Moscow, Energoizdat Publishers, 1981, p. 142.
4. E.B. Hooper, Jr., P. Poulsen, and P.A. Pincosy. J. Appl. Phys., 52, 7027 (1981).
5. K.N. Leung, L.W. Ehlers, and M. Bacal. Rev. Sci. Instrum., 1, 56 (1983).
6. T.S. Green, A.J. Holmes, and A. Walker. Bull. Am. Phys. Soci., 27, 1055 (1982).
7. J. Los, E.A. Overbosch, and J. Van Wunnik. Proc. Sec. Int. Symp. on Production and Neutralization of Hydrogen Ions and Beams, Brookhaven, N.Y., BNL-51304, 1980, p. 23.
8. G.I. Dimov, X European Conference on Contr. Fusion and Plasma Phys., Moscow, 1981, vol. II, p. 35.
9. Yu. I. Bel'chenko, G.I. Dimov, and V.G. Dudnikov. In Proc. Symp. on Production and Neutralization of Negative Hydrogen Ions and Beams, Brookhaven, NY, 1977, BNL-50727, p. 79 (1977). (See also Preprint No. 77-56, Institute of Nuclear Physics, Novosibirsk, 1977.)

10. Yu. I Bel'chenko and V.G. Dudnikov. Preprint 78-95, Institute of Nuclear Physics, Novosibirsk, 1978. Also Journal de Phys., Colloque C7, No. 7, 40, p. C7-501 (1979).
11. Yu. I. Bel'chenko and V.G. Dudnikov. Trudy XV Mezhdunarodnoi konferentsii po yavleniyam v ionizovannykh gazakh (Transactions of the 15th International Conference on Phenomena in Ionized Gases.) Minsk, 1981, part II, p. P-1504.
12. V.L. Komarov and A.P. Strokach. Zhurnal tekhnicheskoi fiziki, 49, 75 (1979).
13. J.G. Alessi and Th. Sluyters. Rev. Sci. Instrum., 51, 1631 (1980).
14. Yu. I Bel'chenko. Preprint 82-54, Institute of Nuclear Physics, Novosibirsk, 1982. Also Fizika Plazmy, 9 (1983), 1219.
15. K.N. Leung and K.W. Ehlers. Rev. Sci. Instrum., 53, 803 (1982).
16. W.K. Dagenhart and W.L. Stirling. Bull. Am. Phys. Soc., 27, 1136 (1982).
17. M.E. Kishinevskii. Zhurnal Tekhnicheskoi Fiziki, 48, 773 (1978).
18. A.N. Apolonskii, Yu. I Bel'chenko, G.I. Dimov, and V.G. Dudnikov. Pis'ma v Zhurnal Tekhnicheskoi Fiziki, 6, 86 (1980).
19. V.G. Dudnikov and G.I. Fiksel'. Fizika Plazmy, 7, 283 (1981).
20. U.A. Arifov. Vzaimodeistvie Atomnykh Chastits s Poverkhnost'yu Tverdogo Tela (Interaction of Atomic Particles with the Surface of a Solid). Moscow, Nauka Publishers, 1968, p. 102.
21. Yu. I. Bel'chenko, V.I. Davydenko, G.E. Derevyankin, et al. Pis'ma v Zhurnal Tekhnicheskoi Fiziki, 3, 693 (1977).